Inorganic Chemistry
Cite This: Inorg. Chem. 2019, 58, 12628−12634
Article
pubs.acs.org/IC

Structural Phase Transition, Optical and Electrical Property Evolutions of Thiospinel $AgIn_5S_8$ under High Pressure

Ting Wen,[†] Qian Zhang,[†] Nana Li,[†] Yonggang Wang,*[,†] Dongzhou Zhang,[‡] Lin Wang,[†] and Wenge Yang*[,†]

[†]Center for High Pressure Science and Technology Advanced Research (HPSTAR), Beijing 100094, China
[‡]Hawaii Institute of Geophysics and Planetology, University of Hawaii Manoa, Honolulu, Hawaii, United States

Supporting Information

ABSTRACT: Thiospinel $AgIn_5S_8$ as a visible-light-active semiconductor has been frequently used as a photoabsorber in solar cells, optoelectronics devices, and photoelectrochemical cells. Similar to temperature, pressure is an efficient external stimulus for both crystalline structural and electronic modulations to improve properties. Herein, we present the pressure tuning effect on $AgIn_5S_8$ up to 40 GPa. A pressure-driven phase transition from the ambient cubic spinel structure to an orthorhombic structure is observed around 10 GPa as evidenced from the in situ high pressure synchrotron X-ray diffraction results. The high pressure phase of $AgIn_5S_8$ adopts the defective $LiVO_2$-type structure with all the Ag^+/In^{3+} cations sitting in the octahedrally coordinated environments. Both the electric transport and photocurrent measurements show dramatic changes along with the phase transition around 10 GPa, and the high pressure phase of $AgIn_5S_8$ exhibits greatly improved conductivity but decreased responses to visible light illumination. Surprisingly, the in situ UV−vis measurements reveal the onset pressure point of bandgap evolution around 7.5 GPa, far below the structural phase transition pressure around 10 GPa, which indicates the early initiated local structural change in the pressure range 7.5−10 GPa. An in situ Raman technique is used to confirm the coordination environment changes of $AgIn_5S_8$ under compression, the results of which reveal the coexistence of both the ambient and the high pressure structure features of $AgIn_5S_8$ in the pressure range 7.5−10 GPa. This work provides a demonstration on how external pressure affects the crystal structure, electronic structure, and optical properties of chalcogenide semiconductors and sheds light on the structure design of better optoelectrical materials under ambient conditions.

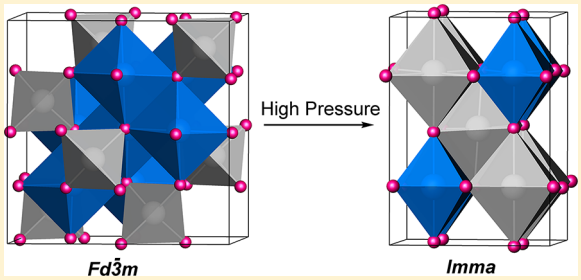

INTRODUCTION

Chalcogenides occur abundantly as minerals in nature and also have attracted intense scientific research attention as semiconducting materials in laboratories. They have been considered as advanced perspective semiconductors exhibiting a broad set of chemical and physical properties and involving a diverse variety of applications, including solar photovoltaics, thermoelectric materials, nonlinear optics, catalysis, electrochemical supercapacitors, superconductivity, etc.[1−6] Additionally, chalcogenides are a chemical class next to organic compounds and metal oxides in compositional and structural diversity. The staggering variety offers us broad opportunities for learning structural insights and acquiring enhanced properties by structural modulations, such as dimensional reduction by chemical exfoliation, local structure distortion by doping, and phase homologies by governing the compositions.[7−9] Besides the various well-demonstrated chemical strategies, pressure is also an efficient tool to tune the crystal and electronic structures by shortening interatomic distances and thus has promise to realize greatly improved physical properties. Many achievements in structural modulations and discovery of hidden phenomena have been acquired through high pressure techniques.[10−13]

Thiospinels, named after the prototype $MgAl_2O_4$, are a type of sulfide with the general formulation $A^{II}B_2^{III}X_4^{VI}$ and crystallize in the cubic crystal system with space group $Fd\bar{3}m$ (no. 227). A partial degree of cation inversion is general in the spinel structure, which has aroused much research interest in the field of high-pressure science for the tunability of the antisite defects under compression.[14,15] Additionally, the fact that phase transition is prone to occur in thiospinels under pressure has brought great attention, and the pressure-driven structural transition has also been studied extensively on compounds with a wide range of chemical compositions.[16] Meanwhile, unusual phenomena such as metal−insulator transition and superconductor−insulator transition were also discovered in thiospinels under high pressure.[17,18]

$AgIn_5S_8$ is one of thiospinel family and can be formulated in the general $A^{II}B_2^{III}X_4^{VI}$ style as $(Ag_{0.5}In_{0.5})In_2S_4$. The crystal structure of $AgIn_5S_8$ can be derived from $CdIn_2S_4$ with Cd replaced by Ag and In atoms.[19] $AgIn_5S_8$ is an n-type semiconductor showing considerable optical responses in the visible light range. Its high-absorption coefficient and suitable

Received: May 9, 2019
Published: September 10, 2019

DOI: 10.1021/acs.inorgchem.9b01351
Inorg. Chem. 2019, 58, 12628−12634

bandgap make it a potential photoabsorber in solar cells, optoelectronics devices, and photoelectrochemical cells.[20−22] So far, there is no scientific research report on $AgIn_5S_8$ under pressure, and its chemical and physical properties under high pressure are still unknown. In this study, we investigated the structural evolution and optical and electrical properties of $AgIn_5S_8$ under high pressure for the first time. Dramatic changes in the electric resistances and photocurrent performance of $AgIn_5S_8$ were observed and associated with the pressure-driven structural phase transition. We also observed abnormal bandgap changes as derived from the optical absorption measurements, which was discussed with the subtle local structure change under high pressure.

EXPERIMENTAL SECTION

Material Synthesis. $AgIn_5S_8$ was synthesized via a solvothermal route by using molten thiourea as the reactive flux. AgCl (0.1434 g, 1 mmol; 99.5%), $InCl_3{\cdot}H_2O$ (1.466 g, 5 mmol; 99.5%), and thiourea ($SC(NH_2)_2$; 2.284 g, 0.03 mol; AR) were weighed and ground together in an agate mortar for several minutes. The mixture was placed in a 50 mL Teflon-lined stainless-steel autoclave and heated at 220 °C for 10 h. An orange powder was obtained after the reaction and washed with ethanol several times. The reddish-brown powder was collected after drying at 80 °C overnight.

Characterization. The phase purity of the as obtained $AgIn_5S_8$ sample was checked with a Bruker D8 Advance diffractometer (Cu Kα source, λ = 0.154 nm) at room temperature and ambient pressure. The composition analysis was performed by energy-dispersive spectra (EDS) using a Quanta 250 FEG FEI Scanning Electron Microscope (SEM).

In-Situ High-Pressure Characterizations. Standard symmetrical diamond-anvil cells (DACs) with 300-μm culets were used in all high-pressure measurements. Stainless steel or rhenium gaskets were preindented to about 40 μm in thickness, and 150 μm holes were drilled using a laser drilling system to serve as the sample chambers. The $AgIn_5S_8$ powder was pressed into a pellet and loaded into the sample chamber filled with silicone oil as the pressure-transmitting medium (PTM). A ruby sphere was then loaded to calibrate the pressure by using the ruby fluorescence method.[23] No PTM was used in the electrical transport measurements.

Powder X-ray diffraction (XRD) patterns were collected at beamline 13 BM-C at the Advanced Phonon Source (APS), Argonne National Laboratory (ANL). A focused monochromatic X-ray beam of about 12 μm × 18 μm in FWHM and a wavelength of 0.4340 Å was used. The diffraction data were recorded with a CCD image plate. High purity CeO_2 powder was used as the standard for calibration. The powder XRD patterns were integrated with the Dioptas program.[24] Lattice parameter refinements were performed by using the FULLPROF program.[25]

Raman spectra were collected using a 532 nm line and a 2400 slits/mm diffraction grating in a Renishaw inVia spectrometer. UV−vis absorption spectrum measurements were conducted using an Ocean Optics QE65000 scientific-grade spectrometer. Transmittance data were recorded, and signals passing through the silicon oil area were used as a background. Resistance measurements were performed using the four-probe method with a 2182A nanovoltmeter, a Keithley 6221 current source, and a 7001 switch system. Photocurrent measurements were performed using a Zennium electrochemical workstation (Zahner) and a 50 W Xe lamp as the light illumination source.

RESULTS AND DISCUSSION

Synthesis and Ambient Crystal Structure of $AgIn_5S_8$. $AgIn_5S_8$ powders were synthesized via a molten thiourea route.[26] The phase purity of the products was preliminarily confirmed by XRD (Figure S1) and energy-dispersive spectra (Figure S2) under ambient conditions. Rietveld refinement of the ambient XRD data was performed, and the result is plotted in Figure 1. The pattern can be well fitted by using the cubic

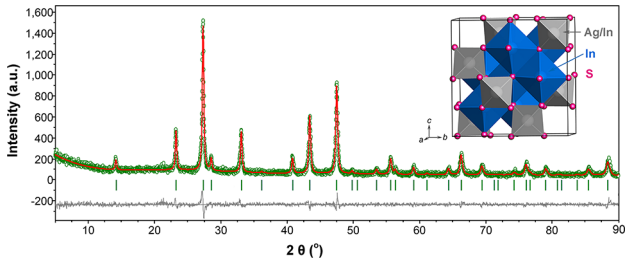

Figure 1. Rietveld refinement plot of $AgIn_5S_8$ at room temperature in space group $Fd\bar{3}m$, $a = b = c$ = 10.8303(2) Å. Green circles: experimental data. Red line: calculated. Green bars: Bragg reflection positions. Gray line: difference. Inset shows the crystal structure of $AgIn_5S_8$ under ambient conditions comprised of $(Ag/In)S_4$ tetrahedra (gray) and InS_6 octahedra (blue).

space group $Fd\bar{3}m$ (No. 227) with cell parameters $a = b = c$ = 10.8303(2) Å. The crystal structure of $AgIn_5S_8$ is shown in the inset of Figure 1. Under ambient conditions, $AgIn_5S_8$ crystallizes in a normal spinel structure, which can be considered as a derivative of $CdIn_2S_4$ with the Cd atom replaced by the Ag/In atom. From the view of structural chemistry, $AgIn_5S_8$ can also be noted as $(Ag_{0.5}In_{0.5})In_2S_4$ to match the general formula of a spinel $A^{II}B_2^{III}X_4^{VI}$. In such a structure, silver and 1/5 of the indium atoms locate disorderly in the tetrahedrally coordinated sites, and the other 4/5 of the indium atoms occupy the octahedrally coordinated positions. The $(Ag/In)S_4$ tetrahedra and the InS_6 octahedra connect each other in a corner-sharing manner.

Pressure-Induced Phase Transition. To explore the structure evolution of $AgIn_5S_8$ under high pressure, in situ powder XRD measurements were conducted up to 42.3 GPa. Figure 2 shows the XRD patterns of $AgIn_5S_8$ as a function of

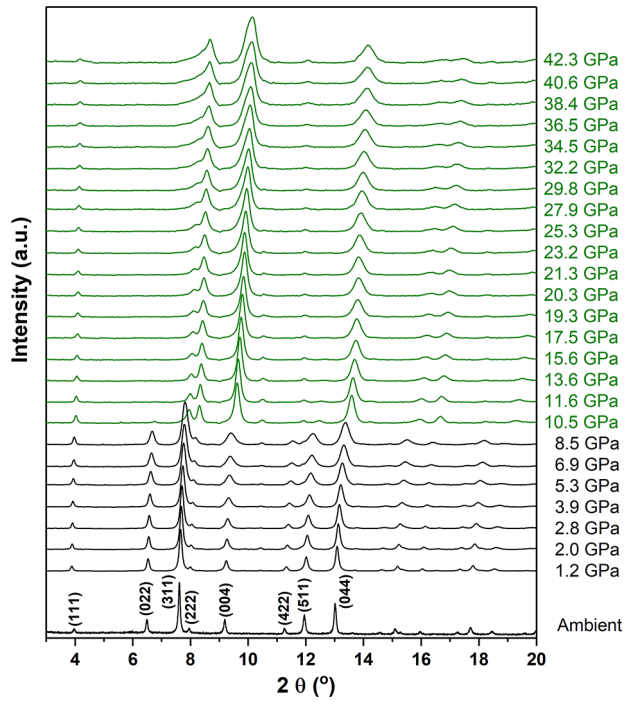

Figure 2. Powder XRD patterns of $AgIn_5S_8$ as a function of pressure.

DOI: 10.1021/acs.inorgchem.9b01351
Inorg. Chem. 2019, 58, 12628−12634

pressure. At ambient pressure and below 10.5 GPa, all the peaks can be well indexed with the cubic space group $Fd\bar{3}m$. As the pressure increases, most of the diffraction peaks shift to higher 2θ values, indicating the contraction of the unit cell and a decrease of the interatomic distances under compression. A structural phase transition occurs at 10.5 GPa as a set of new peaks emerge, and the high pressure (HP) phase can be preserved to up to 42.3 GPa. Moreover, the pressure-induced phase transition of $AgIn_5S_8$ around 10.5 GPa is reversible. After pressure releasing, $AgIn_5S_8$ returns to the original spinel structure (Figure S3).

We found that the XRD pattern of the HP phase of $AgIn_5S_8$ can match that of $LiVO_2$ ($Fd\bar{3}m$) well (Figure S4). The difference between the formulas of $LiVO_2$ ($A^IB^{III}X_2^{VI}$) and the spinel $(Ag_{0.5}In_{0.5})In_2S_4$ ($A^{II}B_2^{III}X_4^{VI}$) can be made up by taking the existence of vacancies into account in a chemical formula $[(Ag_{0.5}In_{0.5})\square]In_2S_4$. Thus, a defective $LiVO_2$-type structure with orthorhombic space group *Imma* (No. 74) is adopted for the structure refinements of the HP-$AgIn_5S_8$.[14,27] Figure 3

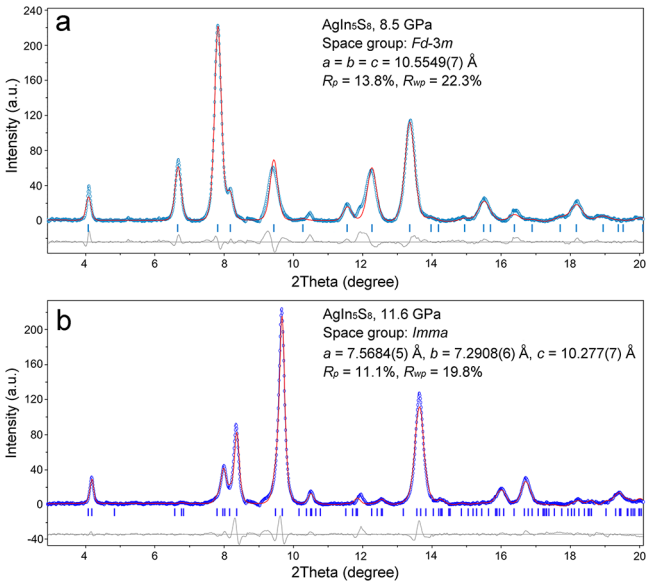

Figure 3. Rietveld refinement results based on the powder XRD data of $AgIn_5S_8$ at selected pressures: (a) 8.5 GPa and (b) 11.6 GPa. The observed, calculated, and difference X-ray diffraction profiles are represented as cyan/blue, red, and gray lines, respectively.

shows the representative powder XRD refinements of $AgIn_5S_8$ at 8.5 and 11.6 GPa, from which the well-fitted plot at 11.6 GPa supports the choice of the defect $LiVO_2$-type structure. Figure 4 presents the crystal structures of $AgIn_5S_8$ before and after phase transition. In the crystal structure of HP-$AgIn_5S_8$, Ag/In atoms occupy the octahedral sites (4*a* in *Imma*) disorderly instead of the tetrahedral sites (8*a* in $Fd\bar{3}m$) in the initial spinel structure. The coordination number of Ag/In increases from 4 to 6, which is reasonable in a pressure-induced phase transition. This also leads to vacancies in the octahedral positions in the same amounts as the Ag/In sites. Accordingly, the Wyckoff positions of In (16*d*) and S (32*e*) atoms in the low pressure (LP) spinel structure change to In (4*b*, 4*c*) and S (8*h*, 8*i*) in the defective $LiVO_2$ structure. Additionally, the defective $LiVO_2$-type structure can also be considered as a partially ordered 2 × 2 × 2 superstructure of the NaCl structure.[27] In the high pressure studies of other spinel-type sulfides such as $CdIn_2S_4$, $MgIn_2S_4$, and $MnIn_2S_4$, a

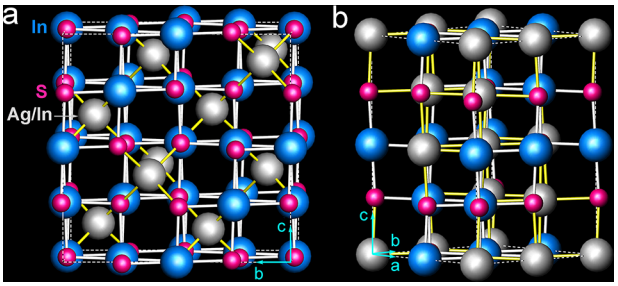

Figure 4. (a) Crystal structure of the ambient phase of $AgIn_5S_8$ with a spinel structure (space group $Fd\bar{3}m$). Pink and blue spheres represent the S and In atoms, respectively. (b) The proposed crystal structure for the HP phase of $AgIn_5S_8$ with defective $LiVO_2$-type structure (space group *Imma*).

similar phase transition was observed, and the HP phase was described using a defective $LiTiO_2$-type structure.[14] In our case, the defective $LiVO_2$-type structure is suitable for HP $AgIn_5S_8$ rather than the $LiTiO_2$-type structure.

Figure 5 presents the cell parameters and volumes of $AgIn_5S_8$ obtained from the fitting of the XRD patterns. The

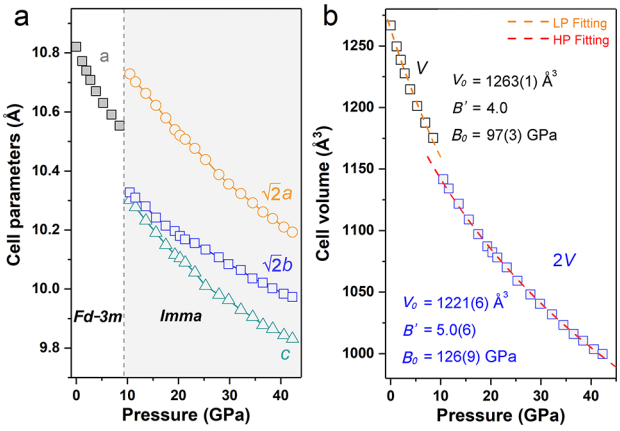

Figure 5. (a) Cell volumes as a function of applied pressure for the LP and HP phases of $AgIn_5S_8$. (b) Cell parameters of $AgIn_5S_8$ as a function of applied pressure.

structural phase transition occurs around 10.5 GPa with a discontinuousness in the cell parameters. The LP to HP phase transition in $AgIn_5S_8$ accompanies a volume decrease by 2.9%, indicating a little more closely packed defective $LiVO_2$ structure. The P−V data were used to fit the equation of state (EOS) using a third-order Birch−Murnaghan method.[28] The results show that the HP phase of $AgIn_5S_8$ (B_0 = 126 GPa) is harder to compress than the LP phase of $AgIn_5S_8$ (B_0 = 97 GPa).

Transport and Optical Properties of $AgIn_5S_8$ under High Pressure. The electrical conductivity and photocurrent are two important characteristics of a semiconductor for practical applications. In situ resistance measurement of $AgIn_5S_8$ was carried out by using four-probe methods within DAC devices to explore the transport behavior of $AgIn_5S_8$ under high pressure. In situ photocurrent was measured using the same setup with Xe light as the light illumination source. Both the resistance and photocurrent are not detected before 7 GPa due to high contact resistance between the Au wires and the powder. Figure 6a shows the electrical resistance as a function of pressure in the range of 7−34.1 GPa. Along with

DOI: 10.1021/acs.inorgchem.9b01351
Inorg. Chem. 2019, 58, 12628−12634

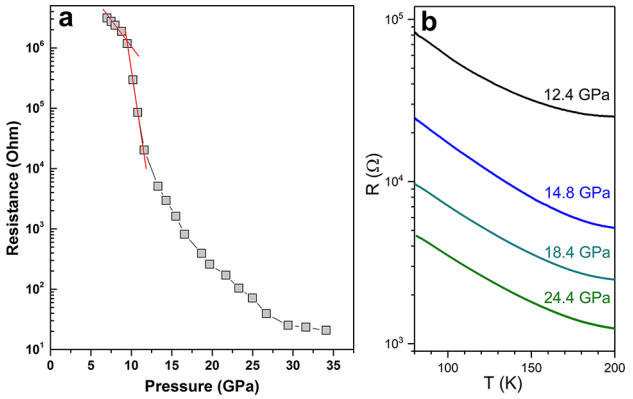

Figure 6. (a) Electrical resistances of $AgIn_5S_8$ as a function of pressure. (b) The temperature dependence of resistance of HP phase $AgIn_5S_8$.

the pressure increase, the electric resistance falls down in the whole measured pressure range by 6 orders of magnitude and drops quickly at approximately 10 GPa, coinciding with the structural phase transition pressure. The temperature dependence of resistance was measured at different pressures for the HP phase of $AgIn_5S_8$ (as shown in Figure 6b), from which typical semiconductor behavior for the HP phase of $AgIn_5S_8$ is evident. In the photocurrent measurements (as shown in Figure 7), $AgIn_5S_8$ shows an obvious response to the on−off switch of the visible light in both the LP and HP phases. The photocurrent intensity falls down dramatically by 3 orders of magnitude from 7 to 10.8 GPa and then decreases slowly up to 34.1 GPa. The evolutions of both the transport and photocurrent intensity are obviously caused by the crystal structure change with the pressure-induced phase transition around 10 GPa.

Bandgap is another important characteristic for a chalcogenide semiconductor. The bandgap evolution of $AgIn_5S_8$ is derived from the optical absorbance data by using the Tauc plot method,[29,30] according to the equation

$$(h\nu\alpha)^{1/n} = A(h\nu - E_g) \quad (1)$$

where h is Planck's constant, ν is the frequency of vibration, α is the absorption coeffcient, E_g is the bandgap, and A is the proportional constant. The value of the exponent n denotes the nature of the sample transition and is theoretically equal to 1/2 or 2 for direct allowed and indirect allowed transitions, respectively.

$AgIn_5S_8$ is a direct bandgap semiconductor despite some debate in previous studies.[31−35] In our study, the optical absorption spectra of $AgIn_5S_8$ at low pressures exhibit a steep absorption, which also confirms the characteristic of a direct bandgap (Figure 8a and b). Thus, n = 1/2 is used for the fitting of the absorbance data to obtain the bandgap values of $AgIn_5S_8$ up to 7.5 GPa. However, the absorption spectra above 8.5 GPa tend to be flat, which is obviously different from the shape at lower pressures. This suggests a direct-to-indirect bandgap transition in $AgIn_5S_8$ along with the structural phase transition under compression. So, n = 2 is chosen to obtain the indirect bandgap values from 8.5 to 13.7 GPa. As shown in Figure 8c, the bandgap value (E_g) of $AgIn_5S_8$ increases linearly upon compression up to 6.9 GPa and decreases sharply from 7.5 to 9.6 GPa, followed by a linear decrease above 10.6 GPa. The bandgap evolution of $AgIn_5S_8$ is inconsistent with the structural phase transition, indicating an early initiated subtle local structure change between 7.5 and 10.6 GPa. Moreover, the bandgap change of $AgIn_5S_8$ under high pressure is reversible upon pressure release.

Raman Spectra of $AgIn_5S_8$ under High Pressure. Raman spectroscopy was used to gain further insight into the local structure change of $AgIn_5S_8$ under high pressure. Figure 9 represents the room temperature Raman spectra of $AgIn_5S_8$ up to 40.5 GPa. At 0.6 GPa, four peaks at wavenumbers 180, 281, 330, and 360 cm^{-1} are observed, which can be assigned to the vibration modes of E_g, F^2_{2g}, F^3_{2g}, and A_{1g} of $(Ag/In)S_4$ tetrahedra.[19] Then, all the Raman peaks shift to higher wavenumbers and the peak intensity increases at the same time up to 7.5 GPa, which can be attributed to the shortening of the (Ag/In)−S bond length under compression. Starting from 8.4 GPa, the Raman intensities, take the F^3_{2g} mode for example, decrease sharply (as shown in Figure 9c). This indicates the starting of tetrahedrally coordinated Ag/In ions migrating to the interstitial sites in the spinel structure. This also marks the

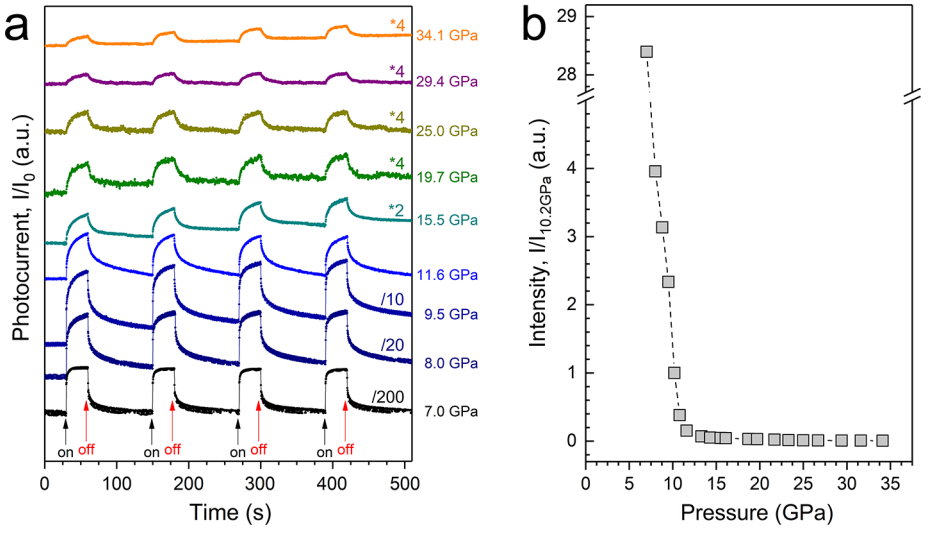

Figure 7. (a) Photocurrent and (b) photocurrent intensities of $AgIn_5S_8$ as a function of pressure.

DOI: 10.1021/acs.inorgchem.9b01351
Inorg. Chem. 2019, 58, 12628−12634

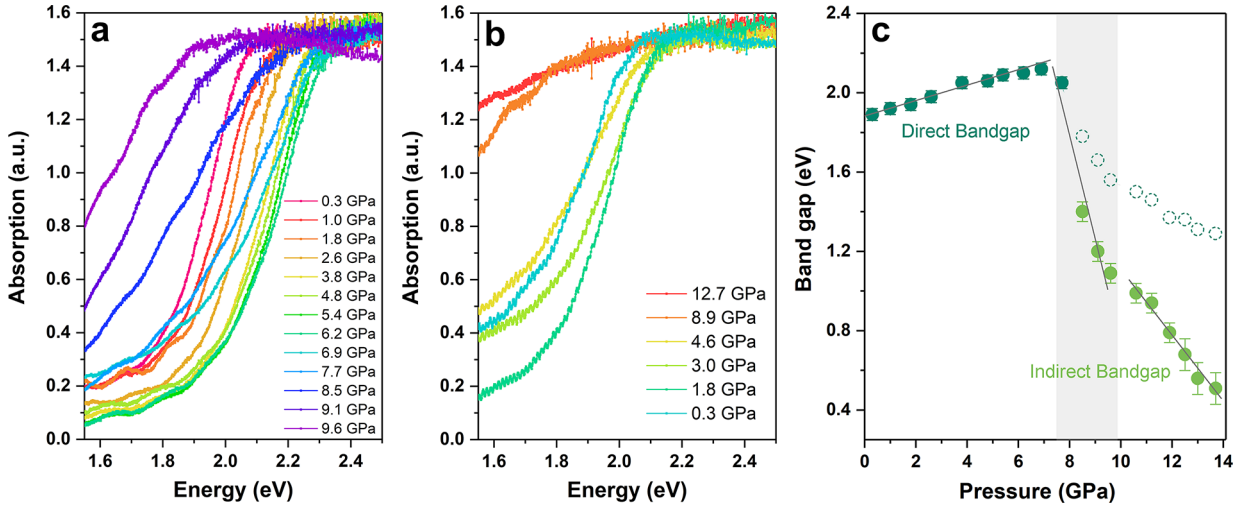

Figure 8. Optical absorption spectra of $AgIn_5S_8$: (a) compression from 0.3 to 9.6 GPa; (b) decompression from 12.7 to 0.3 GPa. (c) Pressure dependence of the bandgap energy for $AgIn_5S_8$. The bandgap values are derived from optical absorbance data by using the Tauc plot method. Solid and empty dark green circles, direct bandgap values; solid light green circles, indirect bandgap values. Solid lines are plotted to lead the eye and do not fit the results.

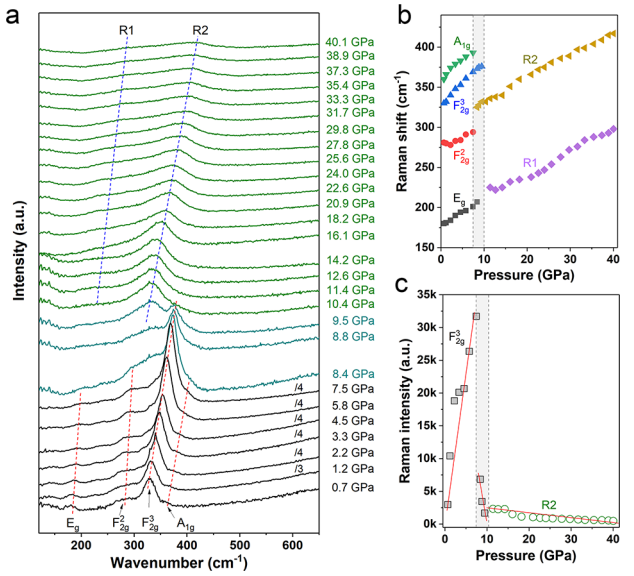

Figure 9. (a) Raman spectra for $AgIn_5S_8$ as a function of pressure. (b) Pressure dependence of the Raman peak positions. (c) Pressure dependence of the peak intensity.

beginning of the phase transition to defective $LiVO_2$-type structure and supports the previous structural analysis results well. Notably, one can consider a coexistence of the LP and HP phases in a pressure range from 8.4 to 9.5 GPa, and the structural phase transformation completes at 10.4 GPa. The local structure evolution as evidenced from the Raman spectra is consistent with the observation of the transitional range between 7.5 and 10.6 GPa from the bandgap data. This is a good demonstration for Raman spectra as a powerful tool to capture subtle local structure changes that are difficult to catch by diffraction techniques. Above 10.4 GPa, no other Raman change has been observed, indicating that the defective $LiVO_2$-type structure of $AgIn_5S_8$ can be kept up to 40 GPa. Indeed, in a stoichiometric $LiVO_2$ structure, Raman peaks are not expected for ideal $(Ag/In)S_6$ or InS_6 octahedra. The emerging broad band with two maxima (denoted as R1, R2) suggests the symmetry breakdown and the existence of vacancies in the octahedrally coordinated sites.[15]

CONCLUSIONS

In summary, we report the pressure modulating of structural, optical, and electrical properties of $AgIn_5S_8$ up to 40 GPa. The in situ powder XRD measurements indicate a structural phase transition around 10.5 GPa from cubic spinel structure to a defective $LiVO_2$ structure with space group *Imma*. Electrical transport and photocurrent behavior of $AgIn_5S_8$ show dramatic changes around 10 GPa, consistent with the pressure-induced structural phase transition. The bandgap values derived from the absorption data show abnormal changes around 7.5 GPa, which indicates a possible direct-to-indirect bandgap transition and a subtle local structure change starting from 7.5 GPa. Raman spectra confirm the early initial local structural evolution and the mixed structural features in a pressure range between 7.5 and 10.4 GPa. Studies on chalcogenide semiconductors under external pressure can provide in-depth understanding of the structure−property relationship and shed light on the structure design of better optoelectrical materials under ambient conditions.

ASSOCIATED CONTENT

Supporting Information

The Supporting Information is available free of charge on the ACS Publications website at DOI: 10.1021/acs.inorgchem.9b01351.

Figures S1−S4 showing the XRD, the EDS of an ambient $AgIn_5S_8$ sample, a comparison of XRD patterns of $AgIn_5S_8$ released from high pressure compression to ambient pressure and the initial sample before compression, and the XRD comparison between HP-$AgIn_5S_8$ and $LiVO_2$ (PDF)

AUTHOR INFORMATION

Corresponding Authors

*E-mail: yonggang.wang@hpstar.ac.cn.
*E-mail: yangwg@hpstar.ac.cn.

DOI: 10.1021/acs.inorgchem.9b01351
Inorg. Chem. 2019, 58, 12628−12634

ORCID

Ting Wen: 0000-0001-6572-0920
Yonggang Wang: 0000-0003-4816-9182
Dongzhou Zhang: 0000-0002-6679-892X
Lin Wang: 0000-0003-2931-7629
Wenge Yang: 0000-0002-1825-2826

Notes

The authors declare no competing financial interest.

■ ACKNOWLEDGMENTS

This work was supported by the National Key R&D Program of China (2018YFA0305900) and National Natural Science Foundation of China (51527801 and U1530402). GeoSoilEnviroCARS is supported by the National Science Foundation-Earth Sciences (EAR-1634415) and Department of Energy-GeoSciences (DE-FG02-94ER14466). The PX^2 program is supported by COMPRES under NSF Cooperative Agreement EAR-1661511. APS is supported by DOE-BES, under contract No. DE-AC02-06CH11357.

■ REFERENCES

(1) Bag, S.; Gunawan, O.; Gokmen, T.; Zhu, Y.; Mitzi, D. B. Hydrazine-Processed Ge-Substituted CZTSe Solar Cells. *Chem. Mater.* **2012**, *24*, 4588−4593.
(2) Bera, T. K.; Jang, J. I.; Song, J. H.; Malliakas, C. D.; Freeman, A. J.; Ketterson, J. B.; Kanatzidis, M. G. Soluble Semiconductors $AAsSe_2$ (A = Li, Na) with a Direct-Band-Gap and Strong Second Harmonic Generation: A Combined Experimental and Theoretical Study. *J. Am. Chem. Soc.* **2010**, *132*, 3484−3495.
(3) Sootsman, J. R.; Chung, D. Y.; Kanatzidis, M. G. New and Old Concepts in Thermoelectric Materials. *Angew. Chem., Int. Ed.* **2009**, *48*, 8616−8639.
(4) Li, X.; Hao, X.; Abudula, A.; Guan, G. Nanostructured Catalysts for Electrochemical Water Splitting: Current State and Prospects. *J. Mater. Chem. A* **2016**, *4*, 11973−12000.
(5) Si, Q.; Yu, R.; Abrahams, E. High-temperature Superconductivity in Iron Pnictides and Chalcogenides. *Nat. Rev. Mater.* **2016**, *1*, 16017−16032.
(6) Theerthagiri, J.; Karuppasamy, K.; Durai, G.; Rana, A. H. S.; Arunachalam, P.; Sangeetha, K.; Kuppusami, P.; Kim, H. Recent Advances in Metal Chalcogenides (MX; X = S, Se) Nanostructures for Electrochemical Supercapacitor Applications: A Brief Review. *Nanomaterials* **2018**, *8*, 256−284.
(7) Kaneti, Y. V.; Tang, J.; Salunkhe, R. R.; Jiang, X.; Yu, A.; Wu, K. C. W.; Yamauchi, Y. Nanoarchitectured Design of Porous Materials and Nanocomposites from Metal-Organic Frameworks. *Adv. Mater.* **2017**, *29*, 1604898−1604938.
(8) Xiao, J.; Yang, S.; Feng, F.; Xue, H.; Guo, S. A Review of the Structural Chemistry and Physical Properties of Metal Chalcogenide Halides. *Coord. Chem. Rev.* **2017**, *347*, 23−47.
(9) Panich, A. M. Electronic Properties and Phase Transitions in Low-dimensional Semiconductors. *J. Phys.: Condens. Matter* **2008**, *20*, 293202−293244.
(10) Baldini, M.; Struzhkin, V. V.; Goncharov, A. F.; Postorino, P.; Mao, W. L. Persistence of Jahn-Teller Distortion up to the Insulator to Metal Transition in $LaMnO_3$. *Phys. Rev. Lett.* **2011**, *106*, 066402.
(11) Wen, T.; Wang, Y.; Li, N.; Zhang, Q.; Zhao, Y.; Yang, W.; Zhao, Y.; Mao, H. Pressure-Driven Reversible Switching between n- and p-Type Conduction in Chalcopyrite $CuFeS_2$. *J. Am. Chem. Soc.* **2019**, *141* (1), 505−510.
(12) Wang, Y.; Zhou, Z.; Wen, T.; Zhou, Y.; Li, N.; Han, F.; Xiao, Y.; Chow, P.; Sun, J.; Pravica, M.; Cornelius, A. L.; Yang, W.; Zhao, Y. Pressure-Driven Cooperative Spin-Crossover, Large-Volume Collapse, and Semiconductor-to-Metal Transition in Manganese(II) Honeycomb Lattices. *J. Am. Chem. Soc.* **2016**, *138*, 15751−15757.
(13) Jaffe, A.; Lin, Y.; Mao, W. L.; Karunadasa, H. I. Pressure-Induced Conductivity and Yellow-to-Black Piezochromism in a Layered Cu−Cl Hybrid Perovskite. *J. Am. Chem. Soc.* **2015**, *137*, 1673−1678.
(14) Santamaría-Pérez, D.; Amboage, M.; Manjón, F. J.; Errandonea, D.; Muñoz, A.; Rodríguez-Hernández, P.; Mújica, A.; Radescu, S.; Ursaki, V. V.; Tiginyanu, I. M. Crystal Chemistry of $CdIn_2S_4$, $MgIn_2S_4$, and $MnIn_2S_4$ Thiospinels under High Pressure. *J. Phys. Chem. C* **2012**, *116*, 14078−14087.
(15) Ursaki, V. V.; Manjón, F. J.; Tiginyanu, I. M.; Tezlevan, V. E. Raman Scattering Study of Pressure-induced Phase Transitions in MIn_2S_4 Spinels. *J. Phys.: Condens. Matter* **2002**, *14*, 6801−6813.
(16) Manjon, F. J.; Tiginyanu, I.; Ursaki, V. B. *Pressure-Induced Phase Transitions in AB_2X_4 Chalcogenide Compounds*; Springer-Verlag: Berlin, Germany, 2014; pp 75−102.
(17) Tang, J.; Matsumoto, T.; Furubayashi, T.; Kosaka, T.; Nagata, S.; Kato, Y. Metal−Insulator Transition of $CuIr_2(S,Se)_4$ under High Pressure. *J. Magn. Magn. Mater.* **1998**, *177*, 1363−1364.
(18) Ito, M.; Hori, J.; Kurisaki, H.; Okada, H.; Kuroki, A. J. P.; Ogita, N.; Udagawa, M.; Fujii, H.; Nakamura, F.; Fujita, T.; Suzuki, T. Pressure Induced Superconductor-Insulator Transition in the Spinel Compound $CuRh_2S_4$. *Phys. Rev. Lett.* **2003**, *91*, 077001.
(19) Gasanly, N. M.; Magomedov, A. Z.; Melnik, N. N.; Salamov, B. G. Raman and Infrared Studies of $AgIn_5S_8$ and $CuIn_5S_8$ Single Crystals. *Phys. Status Solidi B* **1993**, *177*, K31−K35.
(20) Cheng, K.; Huang, C.; Huang, Y.; Chuang, H.; Wu, Y. Photoelectrochemical Performance of Aluminum-doped $AgIn_5S_8$ Electrodes Created Using Chemical Bath Deposition. *Thin Solid Films* **2011**, *520*, 469−474.
(21) Qasrawi, A. F. Annealing Effects on the Structural and Optical Properties of $AgIn_5S_8$ Thin Films. *J. Alloys Compd.* **2008**, *455*, 295−297.
(22) Konovalov, I.; Makhova, L.; Hesse, R.; Szargan, R. Intermixing, Band Alignment and Charge Transport in $AgIn_5S_8$/CuI Heterojunctions. *Thin Solid Films* **2005**, *493*, 282−287.
(23) Mao, H. K.; Xu, J.; Bell, P. M. Calibration of the Ruby Pressure Gauge to 800 kbar under Quasi-hydrostatic Conditions. *J. Geophys. Res.* **1986**, *91*, 4673−4676.
(24) Prescher, C.; Prakapenka, V. B. DIOPTAS: a program for reduction of two-dimensional X-ray diffraction data and data exploration. *High Pressure Res.* **2015**, *35*, 223−230.
(25) Rodriguez-Carvajal, J. Recent Advances in Magnetic Structure Determination by Neutron Powder Diffraction. *Phys. B* **1993**, *192*, 55−69.
(26) Sun, B.; He, J.; Zhang, X.; Bu, K.; Zheng, C.; Huang, F. Synthesis, Crystal Structure and Optical Properties of $K_2Cu_2GeS_4$. *J. Alloys Compd.* **2017**, *725*, 557−562.
(27) Chieh, C.; Chamberland, B. L.; Wells, A. F. A High-Pressure Form of Lithium Vanadium Dioxide − a 2 × 2 × 2 NaCI Superstructure. *Acta Crystallogr., Sect. B: Struct. Crystallogr. Cryst. Chem.* **1981**, *37*, 1813−1816.
(28) Birch, F. Finite Elastic Strain of Cubic Crystals. *Phys. Rev.* **1947**, *71*, 809−824.
(29) Tauc, J.; Grigorovici, R.; Vancu, A. Optical Properties and Electronic Structure of Amorphous Germanium. *Phys. Status Solidi B* **1966**, *15*, 627−637.
(30) Davis, E. A.; Mott, N. F. Conduction in Non-crystalline Systems V. Conductivity, Optical Absorption and Photoconductivity in Amorphous Semiconductors. *Philos. Mag.* **1970**, *22* (179), 903−922.
(31) Manjón, F. J.; Segura, A.; Amboage, M.; Pellicer-Porres, J.; Sánchez-Royo, J. F.; Itié, J. P.; Flank, A. M.; Lagarde, P.; Polian, A.; Ursaki, V. V.; Tiginyanu, I. M. Structural and Optical High-Pressure Study of Spinel-type $MnIn_2S_4$. *Phys. Status Solidi B* **2007**, *244*, 229−233.
(32) Paorici, C.; Zanotti, L.; Romeo, N.; Sberveglieri, G.; Tarricone, L. Crystal Growth and Properties of the $AgIn_5S_8$ Compound. *Mater. Res. Bull.* **1977**, *12*, 1207−1211.

DOI: 10.1021/acs.inorgchem.9b01351
Inorg. Chem. 2019, 58, 12628−12634

(33) Usujima, A.; Takeuchi, S.; Endo, S.; Irie, T. Optical and Electrical Properties of $CuIn_5S_8$ and $AgIn_5S_8$ Single Crystals. *Jpn. J. Appl. Phys.* **1981**, *20*, 505−507.
(34) Cheng, K.; Huang, C.; Pan, G.; Chen, P.; Lee, T.; Yang, T. C. K. Physical Properties of $AgIn_5S_8$ Polycrystalline Films Fabricated by Solution Growth Technique. *Mater. Chem. Phys.* **2008**, *108*, 16−23.
(35) Isik, M.; Gasanly, N. Ellipsometry Study of Optical Parameters of $AgIn_5S_8$ Crystals. *Phys. B* **2015**, *478*, 127−130.

DOI: 10.1021/acs.inorgchem.9b01351
Inorg. Chem. 2019, 58, 12628−12634